

CEP after prism + chirped mirrors compressor

The commercial Femtopower front-end of the laser system is CEP stabilized. The initial CEP drift with the fast and slow feedback active was measured to be 176 mrad for a time of 30 minutes. The integration time on the spectrometer was 1 ms, 20 consecutive spectra are averaged for CEP measurement. After reducing the jitter of the acoustic wave of the AOPDF in the laser system (see next section) we decreased this noise to 100 mrad for a measurement of several hours Fig. 6.23.

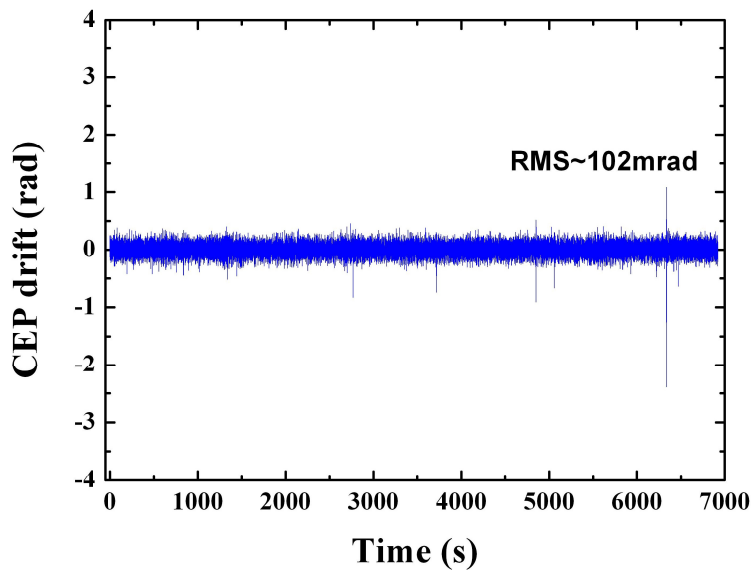


Figure 6.23: Measurement of the CEP drift at the output of the Femtopower. The integration time for each acquisition is 1 ms, 20 consecutive spectra are averaged for CEP measurement.

The same measurement was repeated to characterize the CEP drift between the 4 mJ pulses with the fast loop activated. The measurement trace presented frequent random jumps of the CEP and it was impossible to stabilize the CEP drift with the slow feedback loop. These random variations of the CEP between pulses can not be compensated with the slow feedback loop. We believe that this CEP drift was added by the compressor and in particular by the prisms (the chirped mirrors have been tested separately after the Femtopower without degradation of the CEP). Due to its large dimension (3 meters between the two triplets of prism) the compressor was not sufficiently isolated from the dispersion fluctuation caused by the movement of air between the prism. Probably with a correctly designed cover this problem can be solved. We did not continue in this direction because the propagation in the prisms also strongly degrades the spatial quality of the beam and thus its M^2 . We thus tried a second configuration where the amplified pulses are compressed in a hybrid compressor consisting of transmission gratings and chirped mirrors. The good CEP stabilization we obtained in this configuration and its robustness convinced us to adopt this solution.

6.6 Transmission grating + chirped mirror compressor

The laser setup with the transmission gratings + chirped mirrors compressor is shown in Fig. 6.24. The compressor is composed of two 600 lines/mm, fused silica holographic gratings (Wasatch Photonics). Substituting the prisms with the gratings implies some changes in the laser configuration, primarily due to the fact that the stretcher and compressor are not matched anymore. The prism compressor introduces negative third order dispersion ($-95760fs^3$) and this compensates the positive third order dispersion of the bulk stretcher and the material in the amplifier ($91064fs^3$). In the case of a grating compressor, the third order dispersion is positive and it is therefore added to the value of the stretcher and the material in the amplifier. Furthermore the value of the third order dispersion is directly proportional to the value of the second order dispersion. We decided to compensate all the third order phase with the Dazzler. This is possible only making a trade-off with the negative chirp introduced by the compressor. With a distance between the gratings of 70 mm for an angle of incidence of 13.9° , the spectral phase added by the compressor is $\varphi^{(2)} = -50000fs^2$ and $\varphi^{(3)} = 70000fs^3$. Again the final compression is then achieved after 32 bounces through the negatively chirped mirrors pair. The pulses are thus initially stretched to 7 ps. Decreasing the pulse stretching compared to the previous configuration limits the output pulse energy to 4 mJ. The spectral phase added by the Dazzler in the two compression configurations is reported in Tab. 6.25. The overall transmission of the compression stage is 53 % (60 % for the gratings compressor). Using grooved gratings instead of holographic gratings this efficiency can be increased to 83 %. Temporal and spectral characterization of the 2.1 mJ output pulses was achieved using an home made SPIDER, Fig. 6.26(a),(b), after a DazScope optimization. The spectrum does not exhibit any significant distortions over 100 nm bandwidth. The measured spectral duration is 25 fs, close to the Fourier transform limit. Furthermore, the proposed compression scheme preserves a good spatial quality. ($M^2 = 1.2$). The Gaussian spatial intensity distribution of the focused beam is represented in Fig. 6.26(c).

A few μJ are split off and sent into the collinear f-2f interferometer APS 800, Menlo System to monitor the relative CEP drift of the amplified pulses. Fig. 6.27(a) represents single shot fringe pattern registered at the output of the interferometer (2000 shots, the integration time of the spectrometer is 1 ms). No feedback loop is activated for this acquisition. The visible and well-contrasted interference figure demonstrates the effective CEP stabilization of the laser pulses. This observation is corroborated by the measurement of the corresponding CEP drift on a short time scale (one minute) (Fig. 6.27(b)). The parameters of the APS are: acquisition time=1 ms, cycle loop time =100 ms, 20 consecutive spectra are averaged for CEP measurement. To evaluate the long term stability, the slow drift introduced by the amplifier is then pre-compensated by a feedback loop to the oscillator locking electronics using the measured CEP. Fig. 6.27(c) shows the typical CE phase stabilization of the system with feedback control. The RMS phase error over tens of minutes is 250 mrad. Furthermore we discovered that part of this noise was added by the jitter of the acoustic-wave of the Dazzler (section 6.9). The added CEP noise is in fact linearly proportional to the acoustic wave jitter. In this first configuration the acoustic

rms jitter was measured to be 180-300 ps with a corresponding added CEP noise of 120-220 mrad. Decreasing the acoustic rms jitter to 70 ps noise reduces the added rms phase noise to less than 50 mrad. In this second configuration the measured RMS phase error is 180 mrad (Fig. 6.28) for a measurement of several (3) hours. Comparing this result to the measurement just after the Femtopower (after the Dazzler upgrading) we see that an additional CEP noise close to 80 mrad is added by the second amplifier and the grating compressor.

Small distance between the gratings reduces the sensitivity to beam pointing and air currents in the compressor. In our case, the reduced groove density of gratings and the lower incident angle decrease CEP fluctuations associated with variations of gratings separation (thermal or mechanical drift). Previous studies have theoretically and experimentally demonstrated that the CEP drift stabilization in gratings-based setup may require interferometric control of the effective gratings separation, which nevertheless this introduce additional experimental complexity. In our configuration we overcome this limitation.

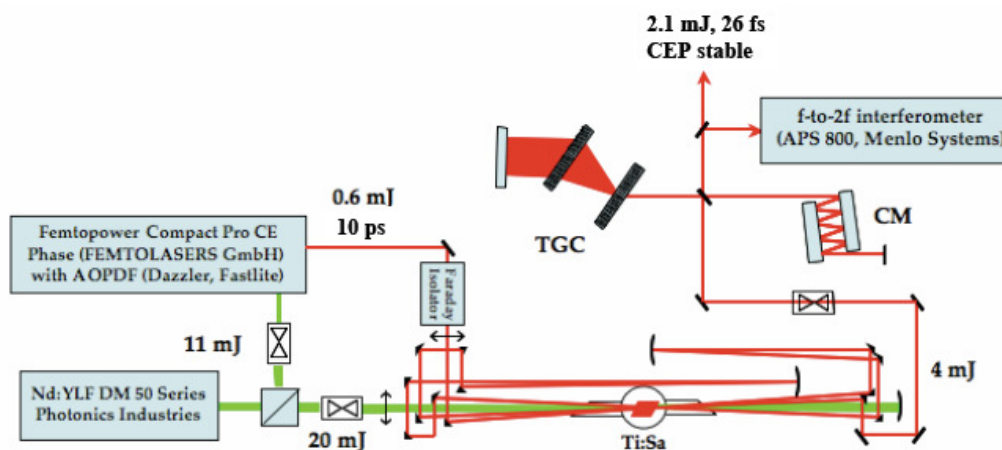


Figure 6.24: Schematic of the 2 mJ, 25 fs, 1 kHz, CEP stable CPA system with transmission gratings and chirped mirror compressor

	Prism compressor +chirped mirrors	Grating compressor + chirped mirrors
$\varphi^{(1)}$ fs	6916	10869
$\varphi^{(2)}$ fs ²	-18464	-30760
$\varphi^{(3)}$ fs ³	25000	-142795
$\varphi^{(4)}$ fs ⁴	-30000	2280

Figure 6.25: Spectral phase added by the Dazzler for the two compressions schemes

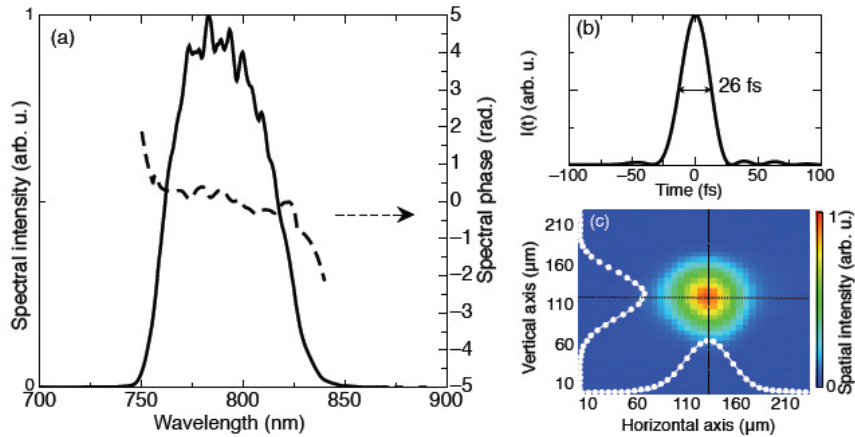


Figure 6.26: Temporal and spatial characterization of the compressed 2.1 mJ pulses. (a) Spectral intensity (solid line) and phase (dashed line) obtained from SPIDER measurement. (b) Temporal intensity profile (SPIDER measurement). (c) Spatial intensity distribution in the far-field (the 7 mm-diameter output beam is focused by a 1 m lens). Vertical and horizontal profiles are fitted by a Gaussian distribution (white lines). The measured value of M^2 factor is about 1.2

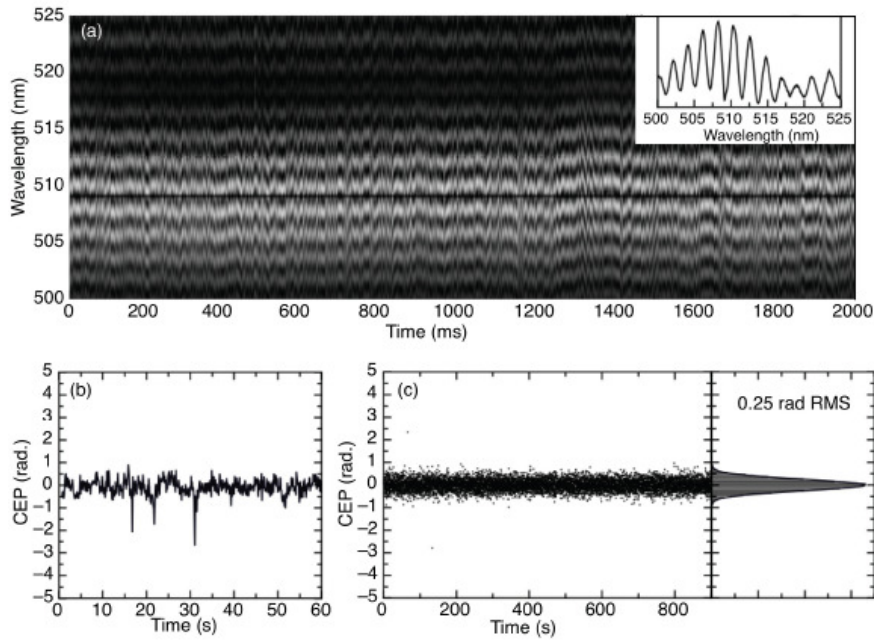


Figure 6.27: CEP stability measurements (spectrometer integration time: 1 ms). (a) Single shot fringe pattern from the collinear f-2f interferometer for 2000 consecutive shots. For illustration one shot is shown in the inset. (b) Measured relative CEP drift of amplified pulses without feedback loop. (c) Measured stabilized CEP drift of amplified pulses with feedback control over 15 minutes (250 mrad RMS). The stabilization of the CEP over an hour has been measured with a RMS error of 290 mrad

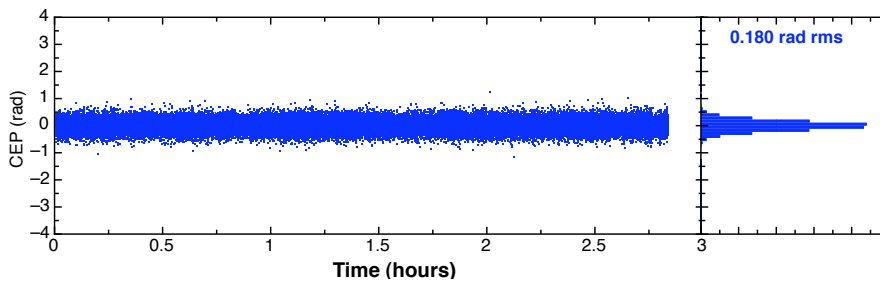


Figure 6.28: Measured stabilized CEP drift of amplified pulses after reduction of the jitter of the acoustic wave of the Dazzler.

6.7 Influence of the B integral on the CEP

The drawback of the small stretching factor of the pulses in the laser system, is the accumulation of a nonlinear phase induced by SPM during amplification. This nonlinear phase is evaluated measuring the B integral of the laser chain. I have shown in section 6.3 how the AOPDF can be used to measure and pre-compensate this spectral phase (DazScope) to avoid its adverse effect on the pulse compression. The B integral is also correlated to the added CEP noise. The intensity fluctuation of the amplified pulse shifts the CEP due to the nonlinear refractive index change. This shift can vary randomly from pulse to pulse and therefore can not be

compensated with an active phase stabilization loop. The refractive index change due to the nonlinear refractive index ($\Delta n = n_2 I$) is $n = n_0 + n_2 I$. The length corresponding to a 2π shift of the CEP is given by:

$$L_{2\pi, nl} = 1/(d\Delta n/d\lambda) = 1/((dn_2/d\lambda)I). \quad (6.8)$$

To make the situation simpler, we assume the intensity I constant over the length L ; then the product of the intensity and the length is given by $IL = \lambda n_0 B_{tot} / 2\pi n_2$. Where B_{tot} , the B integral, is given by expression $B_{tot} = 2\pi / (\lambda n_0) \int_0^L n_2 I dz$. In this case, the CEP shift due to the nonlinear index is given by:

$$\delta\theta_{nl} = 2\pi L / L_{2\pi, nl} = \frac{\lambda n_0}{n_2} \left(\frac{dn_2}{d\lambda} \right) B_{tot}. \quad (6.9)$$

The intensity fluctuation of ΔI results in the fluctuation of the CEP shift of $\Delta\varphi_0 = \delta\theta_{nl} \Delta I$. The list of n_0 , n_2 , $\frac{dn_2}{d\lambda}$ and $\delta\theta_{nl}$ at $B_{tot} = 1$, and the CEP fluctuation for a 1 % intensity fluctuation, is given in Tab. 6.29. For 1 % intensity fluctuation, the CEP fluctuation is on the order of 10^{-3} rad at $B_{tot} = 1$.

Material	n_0 at 800 nm	n_2 (m ² /W)	$dn_2/d\lambda$ (m/W)	$\delta\theta_{nl}$ (rad)	$\delta\theta_{nl} \Delta I$ (rad)
Fused silica	1.45	3.3×10^{-20}	-0.98×10^{-14}	-0.34	-3.4×10^{-3}
Sapphire (n_e)	1.76	3.0×10^{-20}	-1.03×10^{-14}	-0.48	-4.8×10^{-3}

Figure 6.29: List of the parameters related to the CEP shift due to intensity fluctuations

It is thus interesting to effectively measure the B integral of our chain in order to evaluate its contribution on the total CEP noise.

6.8 Measuring the B integral

The B integral of a laser chain can be measured by injecting the amplifier with two delayed pulses and measuring the output replicas of these pulses with a high dynamic range correlator. To understand how two pulses can generate several replicas after amplification and compression

I first give here a short theoretical introduction.

The most intuitive way to understand this temporal "diffraction" is to consider it as a four-wave mixing (FWM) process [2]. As shown in Fig. 6.30, the delay between pulses is chosen so that the pulses partially overlap after the stretching. At any particular position in the overlapped part of the two pulses the instantaneous optical carrier frequencies are ω_1 and ω_2 ($\omega_1 > \omega_2$). Since the pulses are stretched, the instantaneous carrier frequencies are $\omega_1(\tau) = \omega_0 + b(\tau + t_d/2)$ and $\omega_2(\tau) = \omega_0 + b(\tau - t_d/2)$, where t_d is the relative delay. The frequency difference is then $\delta\omega = \omega_1 - \omega_2 = bt_d$. The third order nonlinear polarization,

$$P_{NL} = \chi^{(3)} \left[\tilde{E}_1(\omega_1) + \tilde{E}_2(\omega_2) \right] \left[\tilde{E}_1^*(-\omega_1) + \tilde{E}_2^*(-\omega_2) \right] \times \left[\tilde{E}_1(\omega_1) + \tilde{E}_2(\omega_2) \right] \quad (6.10)$$

gives FWM, SPM and XPM. In particular, the terms $\tilde{E}_1(\omega_1)\tilde{E}_2^*(-\omega_2)\tilde{E}_1(\omega_1)$ and $\tilde{E}_2(\omega_2)\tilde{E}_1^*(-\omega_1)\tilde{E}_2(\omega_2)$ are the FWM process of interest, giving the new frequencies $2\omega_1 - \omega_2$, and $2\omega_2 - \omega_1$. We see that $2\omega_1 - \omega_2 = \omega_1 + bt_d$, so it is constantly blue shifted from $\omega_1(\tau)$. Likewise, $2\omega_2 - \omega_1 = \omega_2 - bt_d$ is red shifted from $\omega_2(\tau)$. When the chirped pulses are recompressed in the compressor, $\omega_1 + \delta\omega = \omega_1 + bt_d$ is advanced by t_d relative to the ω_1 . Because the unshifted frequencies ω_1 collapse to $\tau = 0$ to form the compressed pulse, the blue shifted frequencies will collapse at $\tau = -t_d$ to form the pre-pulse. The same applies to the red shifted post-pulse. The partial overlap causes the bandwidth of the new pulses to be narrower, indeed no time causality is violated.

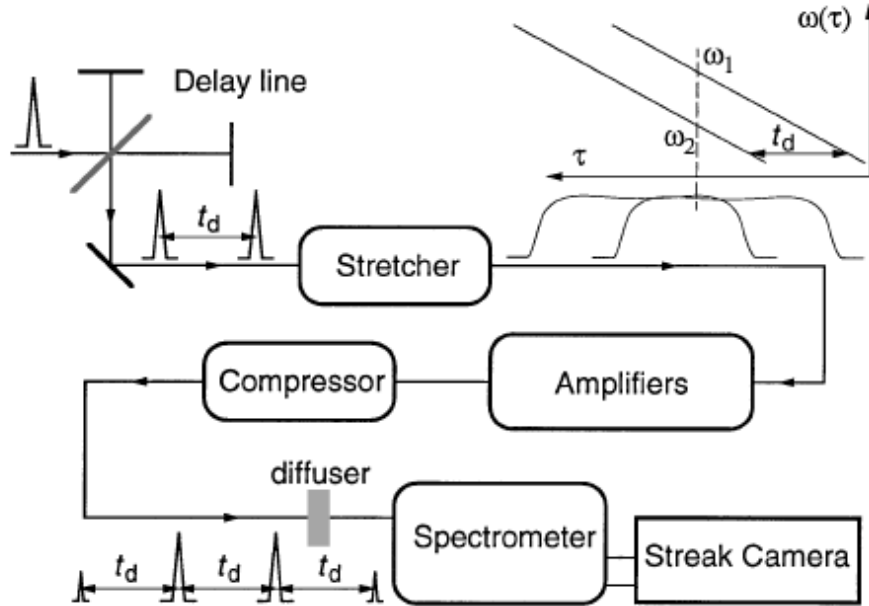


Figure 6.30: Experimental arrangement of nonlinear pulse shaping in a CPA amplifier. Reprinted from [2]

Another valid approach to understand the process is to look at the process as non linear propagation of the composite pulse, which contains the beat pattern. In this picture the new frequencies are generated as a result of SPM. The new frequencies are defined by: $\delta\omega \propto dI(\tau)/d\tau$.

Because of the many rapid intensity oscillations due to the beating, new frequencies are generated efficiently. In particular blue shifted frequencies are generated in the rising fronts and red shifted frequencies in the decreasing front. All the new frequencies generated will interfere in the compressor to give the additional pulses. In particular the amplitude of these replicas compared to the main peak depends of the amount of B integral of the chain. A fit algorithm can then searches for a B integral parameter that minimizes a least-square error function calculated for the temporal sidebands.

In our case two delayed pulses with the same amplitude are generated using the Dazzler present in the first amplifier (so strictly speaking we measure the B integral accumulated after the fourth pass of the first amplifier). The transfer function for generating these pulses is the same as that the one introduced in section 2.3.4 discussing the Phazzler. To measure the output replicas with sufficient dynamic range we used a third order correlator (Sequoia, Amplitude Technologies). In the absence of B-integral, the simulated third order cross correlation shows only three peaks and the energy ratio between the two pulses drives the symmetry of the resulting trace. This point is an important experimental control element; in particular, the relative injection-efficiency of the pulses into the amplifier, whose accurate control is experimentally challenging, can be evaluated that way. In the fit, the energy split ratio is adjusted numerically to fit any experimental asymmetry. In the presence of B-integral, side bands appear and the number and magnitude of the sidebands is adjusted to match the experimental data, using B as fit parameter. A typical measured trace is shown in Fig. 6.31. The multiples replicas separated by the temporal delay T_d are clearly visible. An unexpected asymmetry is visible in the recorded traces. A possible explanation relies on the theory presented previously and is confirmed by the simulation of the replication process. When the spectrum of each individual pulse is numerically isolated, one sees that there is a sizeable frequency shift of the replicas when the pulse-to-pulse delay is comparable to the stretched-pulse width. Experimentally, the delay between the pulses was set to 1 ps, which leads to a frequency shift of 15 nm between the two first replicas at the two side of the main pulses. Such a frequency shift certainly impacts on the conversion efficiency of the measurement setup because of the finite spectral acceptance of the thick frequency mixing crystals in the cross-correlator. The fitted B integral in this case is 1.5 radians. The output energy was reduced in this measurement to avoid any damages in the Ti:Sa crystal. We can then estimate a B-integral of 3 radians at full energy. From Tab. 6.29, the contribution to the CEP noise considering an intensity fluctuation of 2 % is then < 50 mrad.

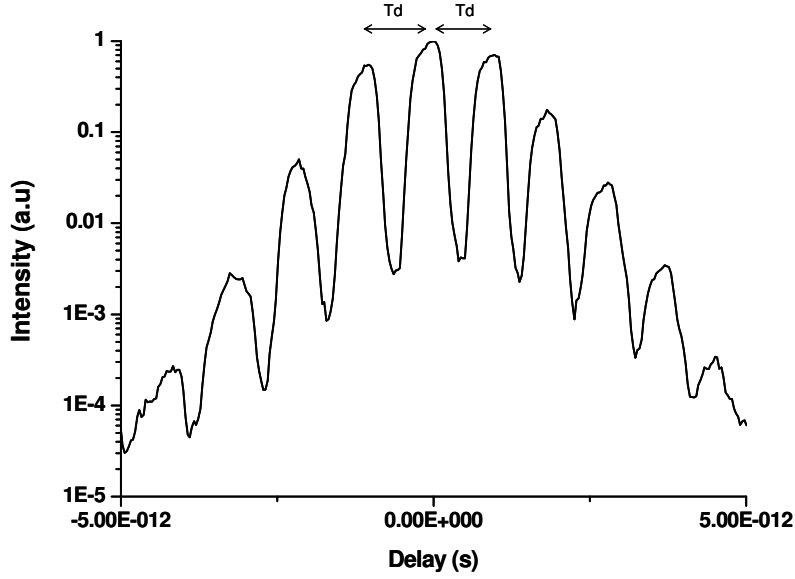


Figure 6.31: Measured high dynamic range correlation (Sequoia) injecting the CPA system with two temporally delayed (T_d) pulses

6.9 Control of the CEP with the Dazzler

Without feedback loop, the CEP drift of the amplified pulses was small enough over several minutes to demonstrate, for the first time, that CEP control could also be performed using the AOPDF inserted in the Femtopower. We do this by controlling the CEP of the acoustic waves in the AOPDF. This first experiment was done before the reduction of the jitter of the acoustic-wave.

The physics of AOPDF is based on a stringent acousto-optic phase-matching relationship between the acoustic and optical wave vectors. As for any phase-matching relationship, this relationship has its counterpart in terms of spectral phase and the acoustic and optical spectral phases are directly linked by the expression :

$$\varphi_{opr,in}(\omega_{opr}) + \varphi_{acc,in}(\omega_{acc}) - \varphi_{opr,diff}(\omega_{opr}) = \pi/2 \quad (6.11)$$

where, $\varphi_{opr,in}$ and $\varphi_{opr,diff}$ are the spectral phase of the input and diffracted optical pulses, and $\varphi_{acc,in}(\omega_{acc})$, is the spectral phase of the acoustic pulse. In this configuration, the electronic generator of the AOPDF is able to control the absolute phase of the acoustic wave within 160 mrad (rms time jitter between the trigger and the RF clock), which translates into the optical domain as follows: the CEP of the diffracted pulse can be changed with respect to the CEP of the input pulse by an arbitrary amount with 160 mrad ($\pi/20$) accuracy. Fig. 6.32 shows the effect of successive CEP jumps of $-\pi$, $+\pi$, $-\pi$, $+\pi/2$, $+\pi/2$, $+\pi/2$, $+\pi/2$ applied by the AOPDF, thereby demonstrating the ability of the AOPDF to exert control over the output CEP. Note here, that the feedback control was turned off to avoid automatic correction of the CEP jumps

by the oscillator locking electronics. These phase steps were performed at a low repetition rate, i.e. not limited by the refresh rate of the AOPDF. By pre-computing and pre-loading a set of RF waves with different CEP values (e.g. 64 waves covering the $0-2\pi$ interval) in SRAM memories, the RF generator is able to change the CEP phase drift at high repetition rate. A demonstration of this achievement is shown in Fig. 6.33 which shows the CEP measured function of time. The word "LOA-ENSTA" was written changing the CEP between successive shots. The vertical segments were obtained by choosing random values of CEP. The baseline (-2.5rad) shows the low CE phase drift of the system during this experiment. This control of the CEP opens the path to closed-loop CEP drift corrections at high repetition rates without any moving parts or retroaction on the oscillator. This is the subject of the next section.

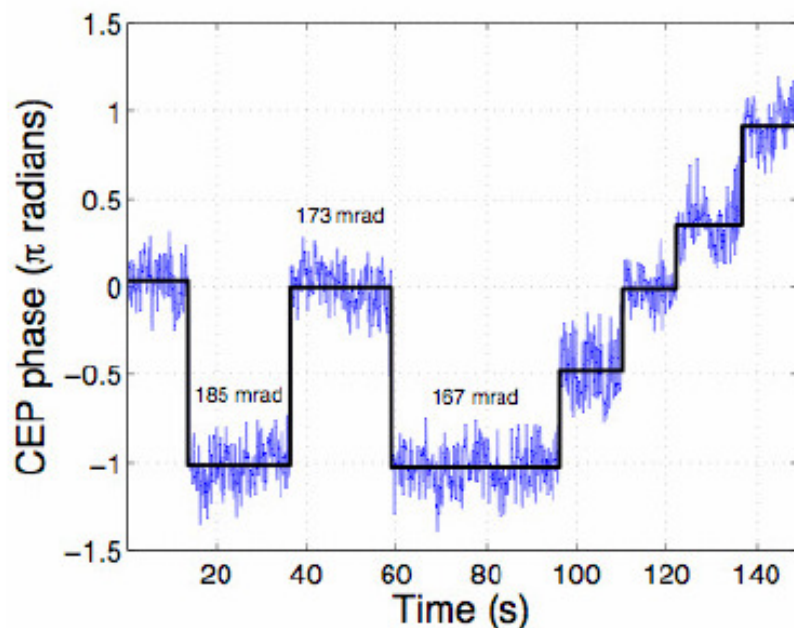


Figure 6.32: Measured CEP (red line) of amplified pulses and successive phase steps applied by the AOPDF (black line). No slow loop feedback was applied

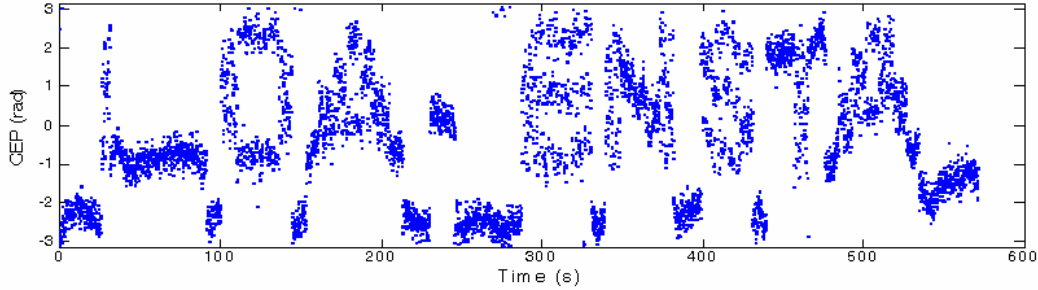


Figure 6.33: Measured CEP function of time. The CEP is changed with the AOPDF at high repetition rate to compose the word "LOA-ENSTA"

6.10 Feedback of the CEP phase with the Dazzler

In the discussion about the CEP stabilization I have explained that, for a correct stabilization of the CEP drift, two feedback loops are needed. A fast feedback loop just after the oscillator and a slow feedback loop at the output of the system for compensating the slow CEP drift caused by the amplifier and the compressor. In the commercial Menlo system both feedback loops act, via an acousto-optical modulator, on the pump intensity of the oscillator. Applying two feedback signals with different time scales on the same actuator is suspected to increase the measured RMS noise on the CEP. This can cause the lock to break earlier than in the undisturbed case producing spikes in the CEP measurement. It is thus interesting to try to separate the two loops. A solution proposed by C.Li et al [1] is to use the signal measured with the $f-2f$ of the slow loops to act with a piezoelectric transducer, changing the distance in the telescope grating of the stretcher. Another solution is to replace the sensitive grating adjustment by the introduction of dispersive material. In particular the CEP of the ultra-short amplified pulses can be controlled by slightly changing the dispersion in the pulse stretcher or compressor, without significantly changing the output pulse duration. In the previous section we have demonstrated how the CEP of the output pulses can be controlled with the AOPDF. This device can then be used to stabilize the CEP after the measurement of the slow drift. The advantage of this solution is the separation of the two loops without any additional elements into the laser chain. The development of this solution has been done in collaboration with Fastlite.

For the CEP stabilization with the AOPDF, like in the commercial APS800 Menlo system, the information from the f-2f fringes is extracted using the FTISI technique. After choosing a target CEP, the correction phase is applied with a proportional-integral (PI) feedback controller with the Dazzler. As discussed previously by pre-computing and pre-loading a set of RF waves with different CEP values in SRAM memories, the RF generator is able correct for any CEP phase drift at high repetition rates. The stabilization repetition rate is in fact determined by the overall loop time. In the case of AOPDF feedback loop this time is 60 ms (10ms of data acquisition, 30ms of data transfer and computation, 20ms of data transfer to RF generator) corresponding to a mean stabilization repetition rate $>15\text{Hz}$. Fig. 6.34 shows the CEP measured with the f-2f interferometer (averaged on 5 shots) before the activation of the AOPDF feedback (firsts 10 seconds) and after the stabilization (64 acoustic wave were loaded). The effect of the feedback is clearly visible. The target of the stabilization was also changed (0,+1,-1,0) to demonstrate the control of the CEP in closed loop. Fig. 6.36 shows the phase noise (dB , rad^2/Hz) for the open loop measurement (blue curve) and after the stabilization with the AOPDF (red curve). The effect of the correction is clearly visible (the intersection of the two curves). The rms CEP stability obtained with the AOPDF feedback loop is 144 mrad (334mrad FWHM) that needs to be compared with the result obtained using the standard APS800 Menlo system loop (131mrad (290mrad FWHM)). The two results are comparable. The large discretization level (98mrad for 64 waves loaded) of the CEP correction in the AOPDF loop is suspected to contribute to the slightly higher rms noise with the AOPDF loop. Future developments will enable a direct hardware feedback on the AOPDF and an increased number of memories (256), allowing both faster (500Hz) and finer ($<25\text{mrad}$) feedback.

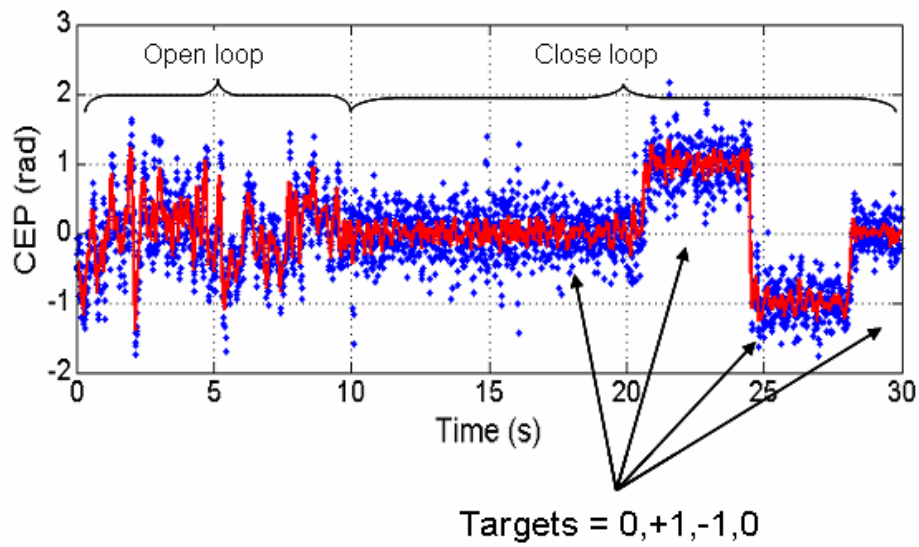


Figure 6.34: Single shot CEP measured with the f-2f interferometer before the activation of the AOPDF feedback (firsts 10 seconds) and after the stabilization. The effect of the feedback is clearly visible. The target of the stabilization was also changed (0,+1,-1,0) to demonstrate the control of the CEP in closed loop

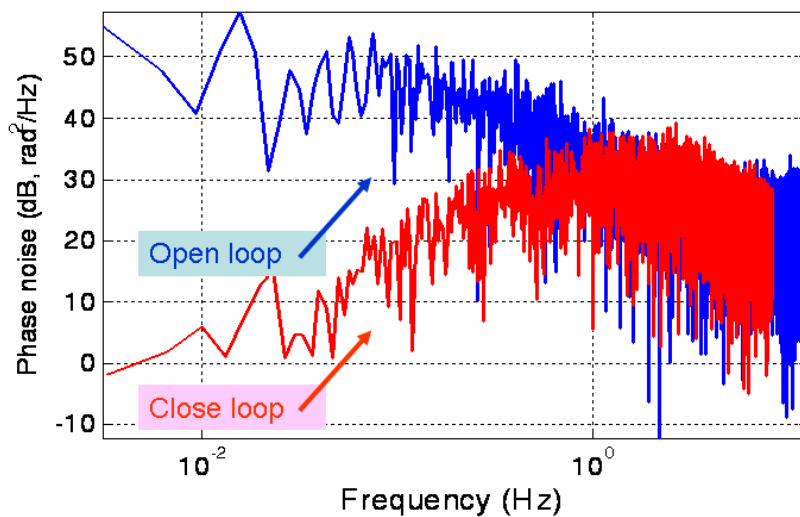


Figure 6.35: Phase noise (dB, rad^2/Hz) for the open loop measurement (blue curve) and after the stabilization with the AOPDF (red curve). The effect of the correction is clearly visible to a frequency of 4 Hz (the intersection of the two curves).

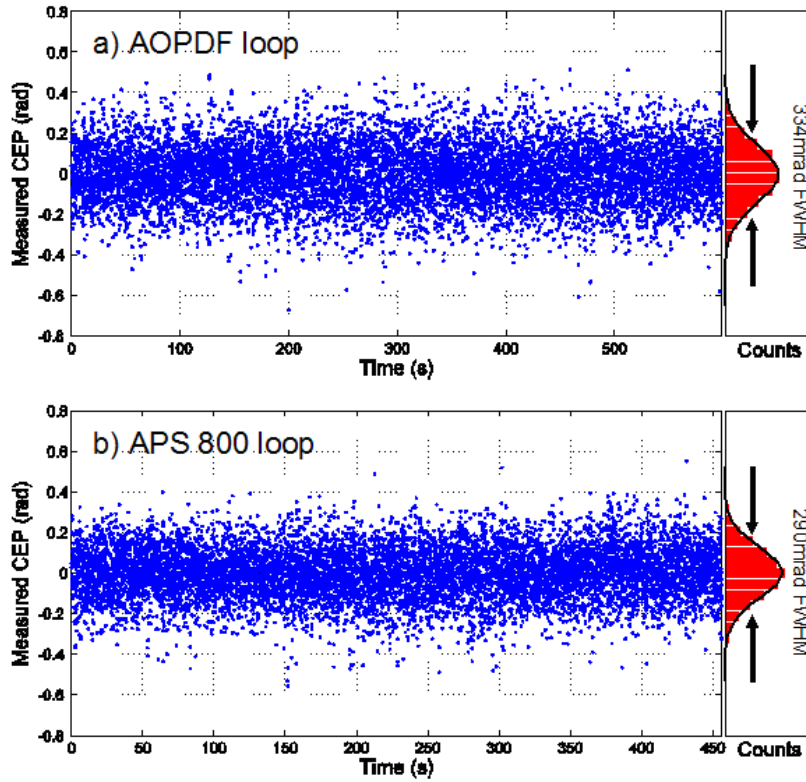


Figure 6.36: Comparison between closed loop operation using the AOPDF (a) or the Menlo loop (b) to correct for the CEP drift. Dots: CE phase values used for correction feedback.

Bibliography

- [1] C. Li, E. Moon, and Z. Chang. Carrier-envelope phase shift caused by variation of grating separation. *Opt. Lett.*, 31(21):3113–3115, 2006.
- [2] X. Liu, R. Wagner, A. Maksimchuk, E. Goodman, J. Workman, D. Umstadter, and A. Migus. Nonlinear temporal diffraction and frequency shifts resulting from pulse shaping in chirped-pulse amplification systems. *Opt. Lett.*, 20(10):1163–1165, 1995.

6.11 Hollow Fiber

6.11.1 Introduction

The temporal duration of the pulses that can be generated in a CPA laser system is limited to approximately 18 fs [15, 7, 22, 20], for mJ level pulses. This limitation is mainly due to the gain narrowing during amplification. To balance this spectral narrowing several spectral shaping techniques have been tested. These solutions make it possible to reach temporal duration shorter than 15 fs. To generate pulses in the few-cycle regime post-compression spectral broadening techniques are necessary. The two most common are the propagation in a hollow-core fiber filled with noble gas [11] and filamentation [9]. Although a higher transmission efficiency and the possibility of self-compression has been claimed for filamentation [17, 8], the main drawback of this technique is that the compressed temporal duration varies radially across the beam [6, 21]. This implies that, in order to obtain a sub-10 fs pulse, only the central part of the beam needs to be selected with a corresponding substantial reduction of the usable energy. Furthermore 5 fs pulses can not be generated in a single filamentation stage. The solution chosen for the "salle noire" laser system is spectral broadening in a hollow fiber.

6.11.2 Hollow fiber

Few-cycle pulses can be generated by extra-cavity compression techniques, in which the pulses are spectrally broadened upon propagation in a suitable nonlinear waveguide and subsequently compressed in a carefully designed optical dispersive delay line. Spectral broadening of laser pulses by self-phase modulation in a single mode optical fiber is a well-established technique: pulses down to 6 fs were obtained in 1987 from 50-fs pulses generated in a mode locked dye laser [5]. More recently 13-fs pulses from a cavity-dumped Ti:sapphire laser were compressed to 5 fs with the same technique [1]. However, the use of a single-mode fiber limits the pulse energy to a few nanojoules. A powerful pulse compression technique based on spectral broadening in a hollow fiber filled with noble gas has demonstrated the capability of handling high energy pulses (sub-mJ range) [11, 12]. This technique presents the advantages of a guiding element with a large diameter mode and a fast nonlinear medium with a high threshold for multiphoton ionization. The theoretical principles of the propagation in a hollow fiber are briefly presented in the next section. In section 6.11.4 I present results about the generation of few-cycle pulses (4.3 fs) with an energy of 1 mJ. The CEP stabilization of this pulses is also demonstrated.

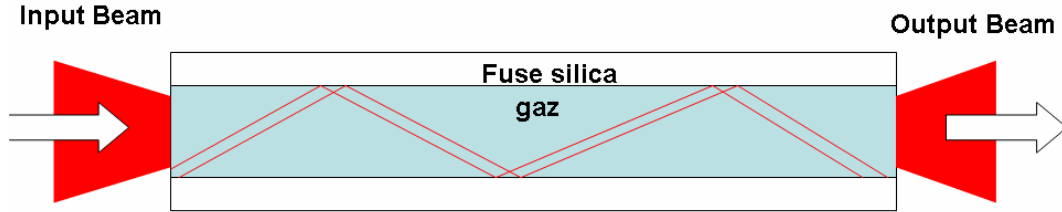


Figure 6.37: Schematic of the propagation in a hollow-core fiber.

6.11.3 Propagation modes and losses in hollow fibers

The use of hollow fibers permits the exploitation of spatially uniform SPM and overcomes the limitation imposed on the pulse energy by the small core diameters of single mode fibers. Owing to the large and scalable mode size, this technique can handle much higher pulse energies than traditionally used single-mode optical fibers. Wave propagation along a hollow waveguide can be thought of as occurring by grazing incident reflections at the dielectric inner surface. Since the losses caused by these multiple reflections discriminate against higher order modes, only the fundamental mode will be transmitted through a sufficiently long fiber. This offers the potential for using a large channel diameter without compromising the quality of the output beam. The modes of hollow cylindrical fibers with diameter much larger than the wavelength were considered by Marcantili and Schmeltzer. These fibers support three types of modes: transverse circular electric (TE_{0m}), in which the electric field lines are transverse concentric circles centered on the propagation axis. Transverse circular magnetic (TM_{0m}), with the electric field directed radially, and hybrid mode EH_{pm} ($|p| \geq 1$) with all the electric and magnetic components present. For fused silica gas-filled fibers the lowest-loss mode is the EH_{11} hybrid mode, whose intensity profile as a function of the radial coordinate r is given by:

$$I(r) = I_0 J_0^2(2.405r/a) \quad (6.12)$$

where I_0 is the peak intensity, J_0 is the zero-order Bessel function and a is the capillary radius. Fig. 6.38 shows the transmission of the fundamental mode EH_{11} at 780 nm as a function of hollow fiber length for different values of the capillary radius.

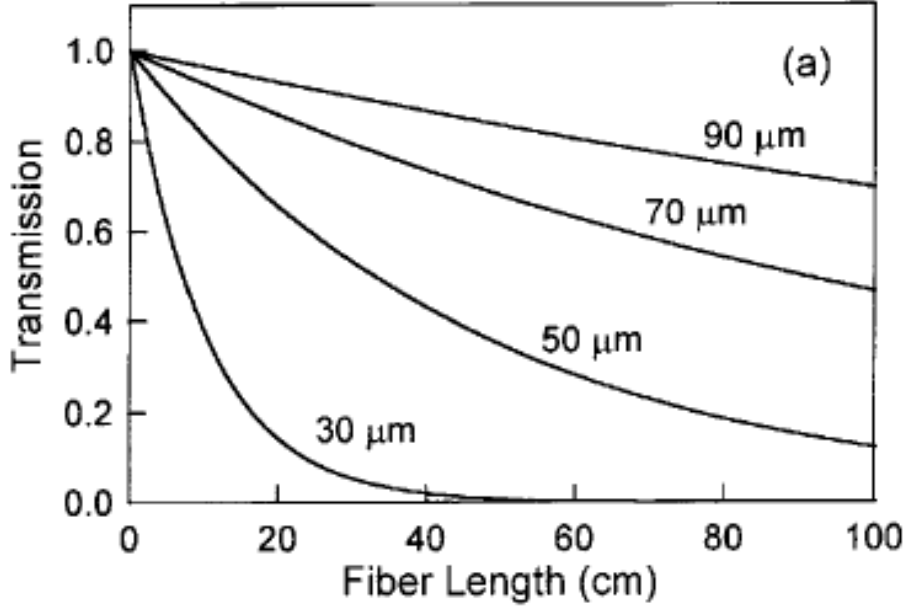


Figure 6.38: Transmission of the fundamental mode EH_{11} at 800 nm function of the fiber lengths and for different internal radius of the fiber. Reprinted from [12].

Another important point is the coupling efficiency of the input power in the fundamental mode EH_{11} . For maximizing this parameter the size of the beam at the input of the fiber needs to match the mode we want to couple. A theoretical coupling efficiency of 90 % has been theoretically demonstrated for a radius between $0.49a$ and $0.84a$. If the modes are not matched the losses increases and more energy is coupled in the higher order modes. This decreases the throughput of the fiber and affects the output spatial quality. Working with a correct coupling, the fiber acts like a spatial filter and the output beam has a very good spatial quality.

The propagation in a hollow fiber is described by the propagation equation I have derived in the SEWA approximation (section 3.4.6). The two main phenomena governing the propagation are SPM and GVD. SPM induces the spectral broadening and introduces a nonlinear spectral phase. The influence of SPM is evaluated defining the non linear length:

$$L_{nl} = \frac{1}{\gamma P_0} \quad (6.13)$$

where P_0 is the peak power of the pulse and γ is the non linear coefficient. γ is defined as:

$$\gamma = \frac{n_2 \omega_0}{c A_{eff}} \quad (6.14)$$

where ω_0 is the laser pulsation, c the speed of light, n_2 the non linear index of refraction of the gaz and A_{eff} the effective area of the mode.

The influence of the GVD is estimated defining the dispersion length L_d :

$$L_d = \frac{T_0^2}{|\beta_2|} \quad (6.15)$$

where T_0 is the duration (at $1/e^2$ in intensity) of the input pulse and $\beta_2 = \frac{\partial^2 \beta}{\partial \omega^2}$ is the dispersion of the group velocity. These two parameters quantify the physical length for the

contributions of SPM and dispersion. In particular for a good compressibility of the spectrally broadened pulses there should be an equilibrium between the two phenomena. The optimal regime is given for a fiber length: $L_{opt} \geq \sqrt{6L_{nl}L_d}$.

6.11.4 Experimental results

Recently, Cavalieri *et al.* have demonstrated sub-4 fs pulses with 400 μ J energy via HCF compression of 1 mJ, sub-23 fs pulses [4]. Additional efforts have been made to push the output energy up to ~ 1 mJ by safely coupling higher energy seed pulses into the fiber [19, 10]. For a HCF filled with a static gas pressure, however, the achievable output energy becomes quickly limited by self-focusing and plasma formation due to ionization of the gas, which degrade beam coupling into the fiber and result in significant energy losses. The use of longer and larger fiber cores with a pressure gradient helps delay these effects until the pulses are coupled well into the fiber, thereby making it possible to scale few-cycle pulse production beyond the mJ level [18, 13, 2].

Spectral broadening in a HCF is strongly dependent on the input pulse parameters such as duration and energy. A much less explored experimental parameter, however, is laser polarization [16]. Changing the polarization state of the laser from linear to circular provides a simple way of coupling more energy into the fiber since it reduces both the Kerr nonlinearity [3] and ionization [14] of the gas at equivalent intensities. The solution we tested to increase the energy out of a statically filled HCF was therefore to seed it with circularly polarized laser pulses. With this technique, we generated 4.3 fs, 1 mJ pulses, compressed from 2.5 mJ, 22 fs seed pulses. A comparison between linear (LP) and circular polarization (CP) shows that the energy throughput and the long-term spectral stability of the output pulses is significantly enhanced for CP.

The high-energy seed pulses in our experiments were generated using the "salle noire" laser at first with prisms + chirped mirrors compressor. The CEP stability after the hollow fiber for this high energy seeding has been confirmed after the installation of the transmission gratings + chirped mirrors compressor.

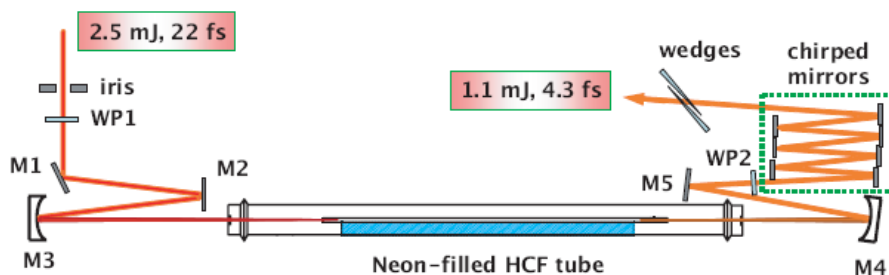


Figure 6.39: Schematic of the statically filled HCF setup seeded with circularly polarized pulses. WP1,2: broadband zero order quarter wave plates.

In the HCF compression setup, shown in Fig. 6.39, the input beam can be changed from LP to CP using a zero-order quarter wave plate (WP1). The beam is then loosely focused into the HCF by a $f = 1.5$ m focusing mirror. The HCF is 1 m long with an inner diameter of $250 \mu\text{m}$ and rests inside a tube filled with a static pressure of Neon gas. The output beam can then be changed from CP back to LP for measurements downstream using a broadband zero-order quarter wave plate (WP2). Residual pulse dispersion is finely compensated by a set of broadband chirped mirrors (CMs) (Femtolasers GmbH) and a pair of fused silica wedges.

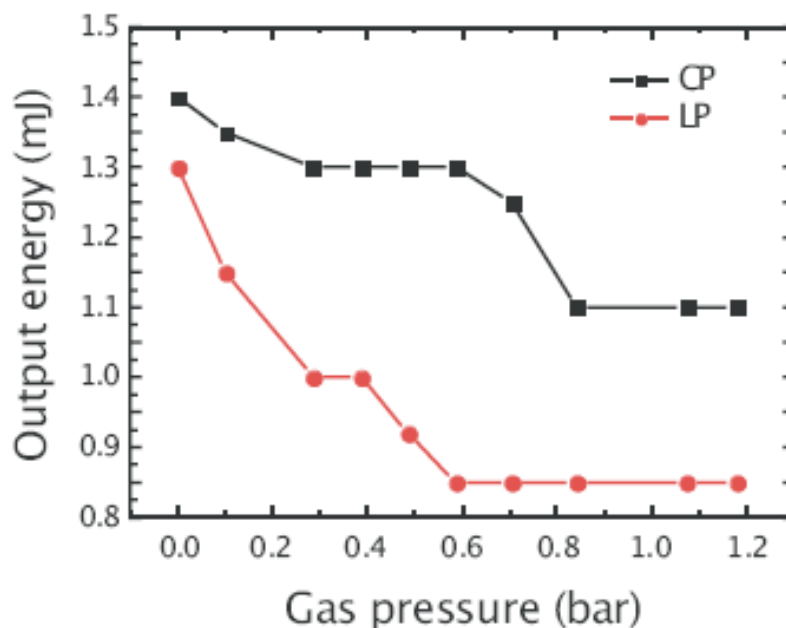


Figure 6.40: HCF output pulse energy for CP (black line) and LP (red line) as a function of Neon pressure, for an input pulse energy of 2.5mJ.

In the experiment, the difference in output pulse energy and spectral broadening between LP and CP was measured for the 2.5 mJ, 22 fs seed pulses. Fig. 6.40 shows the output pulse energy after the HCF as a function of gas pressure. A throughput enhancement is already quite visible for CP even in the case where the remnant gas pressure is very low ($\ll 1$ mbar). For both CP and LP, the output energy decreases with increasing gas pressure but the energy throughput remains higher for CP. Reduced self-phase modulation due to a diminished Kerr effect for CP means that spectral broadening is less pronounced for CP at pressures below ~ 1 bar. At higher pressures, however, pulse broadening for CP becomes comparable to that for LP, which can be explained by higher ionization losses for LP due to stronger ionization. At an optimum pressure of ~ 1.1 bar, the 1.1 mJ output energy measured for CP is almost 30 % higher than the 0.85 mJ measured for LP. Fig. 6.41 shows the spectral broadening recorded for CP and LP at the optimum pressure of 1.1 bar. A careful comparison of the two cases reveals that for CP (black line) a more homogeneous pulse broadening occurs around the central wavelength (780 nm) together with a clear extension of the spectrum towards shorter wavelengths, which is more adapted for obtaining cleaner compressed pulses.

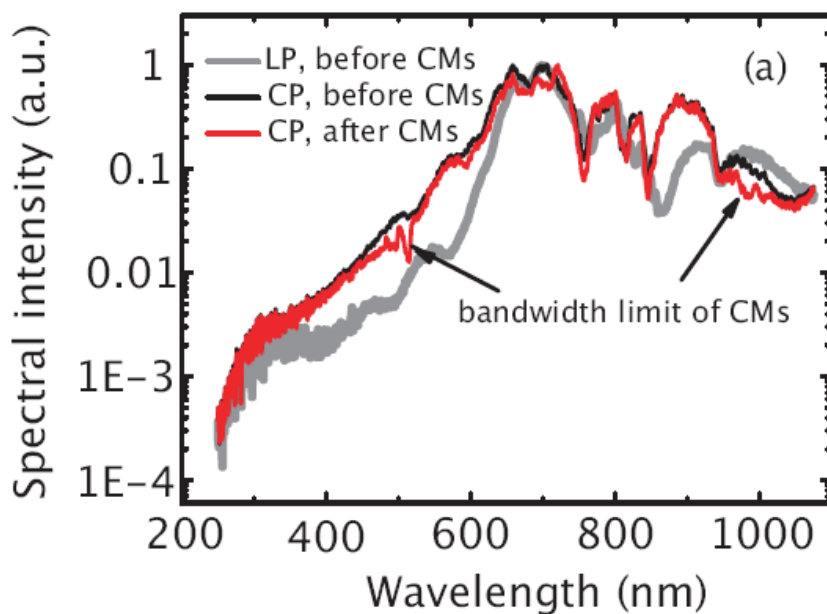


Figure 6.41: Broadened HCF spectrum before (black line) and after (red line) the chirped mirrors for CP and LP before the chirped mirrors (grey line).

At the optimum pressure of ~ 1.1 bar, the broadened spectrum (Fig. 6.41) for CP can support 3 fs transform-limited pulses. The compressed pulse duration is measured after fine compensation of pulse chirp using a commercial second-order autocorrelator (Femtolasers GmbH) suited for sub-5 fs pulse characterization. A typical optimized compression result for CP is shown in Fig. 6.42, showing a very good agreement with the theoretical autocorrelation trace for a 4.3 fs sech^2 pulse at a central wavelength of 780 nm (red filled circle in Fig. 6.42). This pulse duration corresponds to ~ 1.6 cycles of the carrier wavelength. The background oscillations present in the experimental autocorrelation trace are most likely due to satellite pulses resulting from the

combined effects of residual uncompensated spectral phase and the sharp modulations in the broadened spectrum. In addition, spectral clipping due to the bandwidth limit of the chirped mirrors was observed, as shown in Fig. 6.41 (red line), meaning that the compressed pulses could be shorter. Here, it is worth mentioning that the bandwidth of the zero-order quarter wave plate after the HCF is broad enough such that no spectral effects were observed.

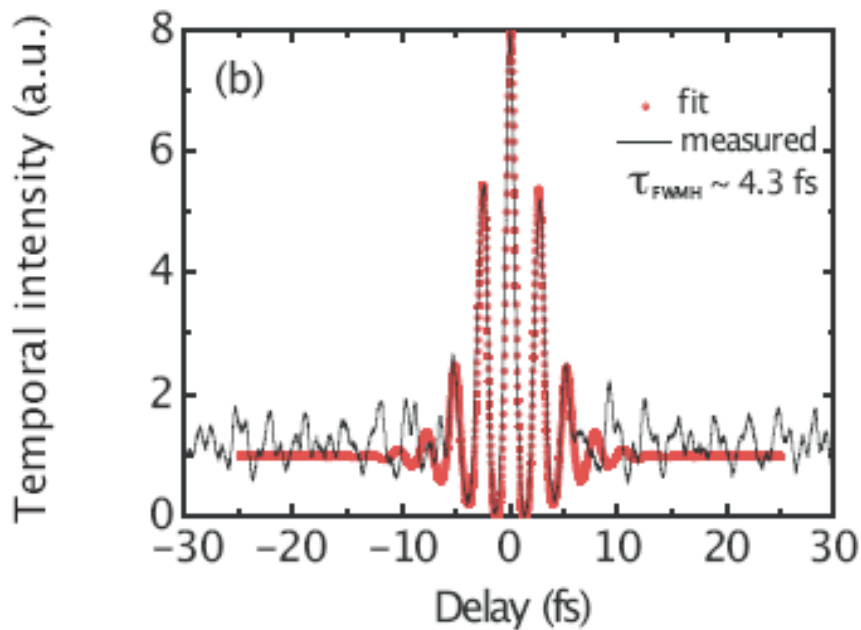


Figure 6.42: Measured (black line) and fitted (red filled circles) second order autocorrelation traces of the compressed pulses for CP. The seed energy is 2.5 mJ and the Neon pressure is 1.1 bar.

Although no obvious differences were observed in beam pointing for both polarization states, we did however observe that CP yields a more stable output spectrum over time. Fig. 6.43 shows density plots of the output spectra for CP and LP made from 20000 successive shots at the optimum pressure of 1.1 bar. Here, we observe a significant improvement in stability for CP, especially at the extremities of the spectrum.

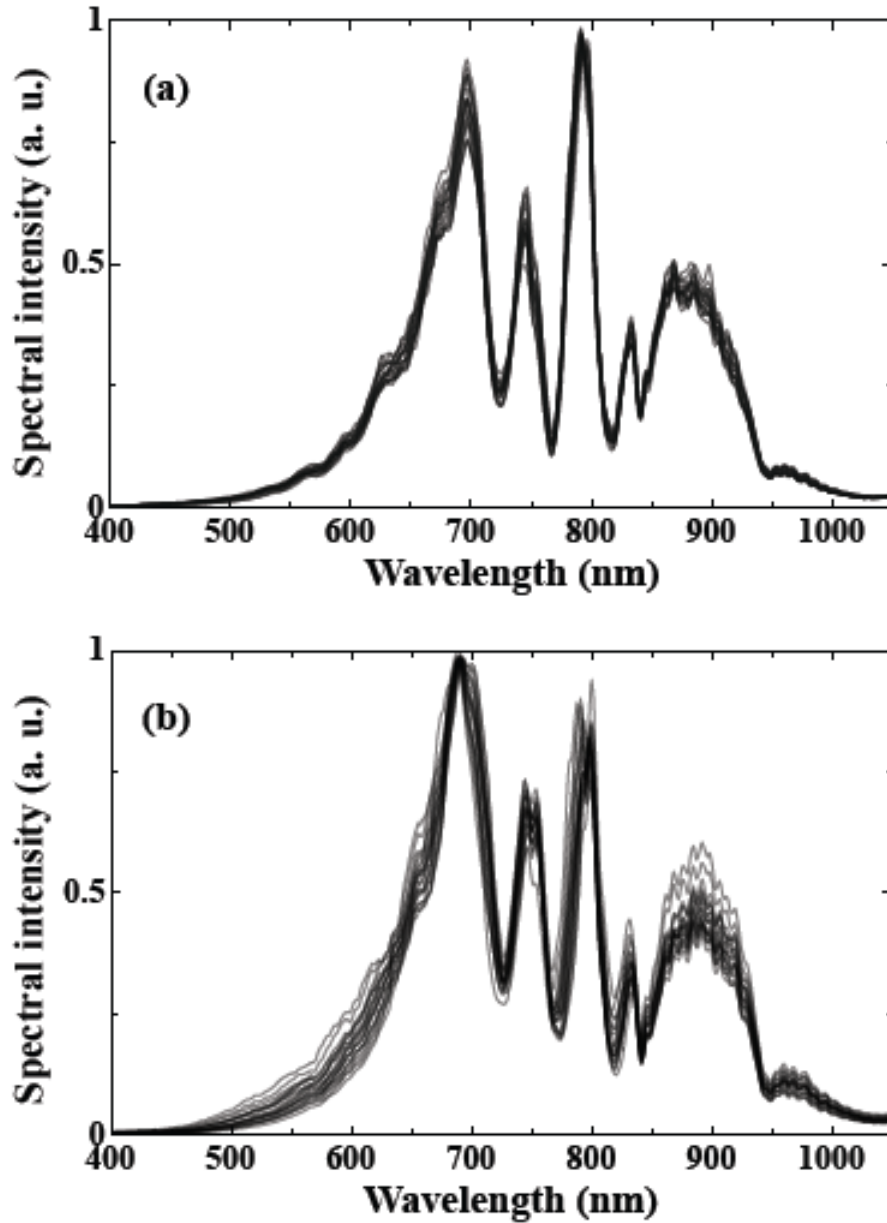


Figure 6.43: Density plot of the output spectrum of the HCF for CP (a) and LP (b) for a seed pulse energy of 2.5 mJ and Neon pressure of 1.1 bar. The fluctuations of the spectrum are the highest where the curve is the broadest

The CEP drift of the compressed pulses was measured with the f-2f interferometer, after the installation of the transmission gratings + chirped mirrors compressor. In this configuration we inject the fiber with 2 mJ with an output of 1.1 mJ. The gas pressure in CP is 1.5 barr. The measured FROG trace of the compressed pulses together with the reconstructed temporal shape is shown in Fig. 6.44. After the fiber the spectrum is already sufficiently broad to be doubled directly in the BBO crystal without passing in the sapphire plate. We measured an RMS CEP drift of 230 mrad (acquisition time 1 ms, averaging on 20 shots) (Fig. 6.45). This corresponds to an additional noise of 50 mrad compared to the results directly after the hybrid compressor. This additional noise is due to the intensity fluctuations that are coupled to CEP

fluctuations by the nonlinear index in the HCF.

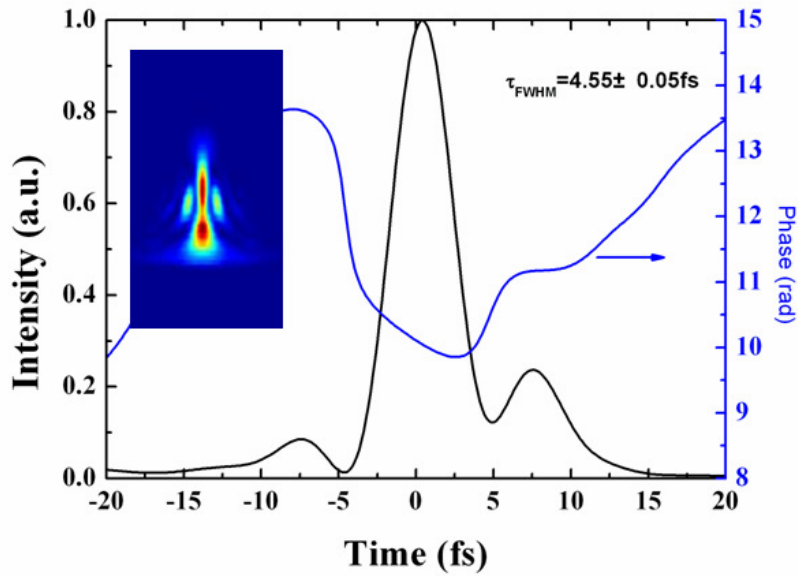


Figure 6.44: FROG trace and temporal reconstruction of the compressed pulses after the hollow-core fiber.

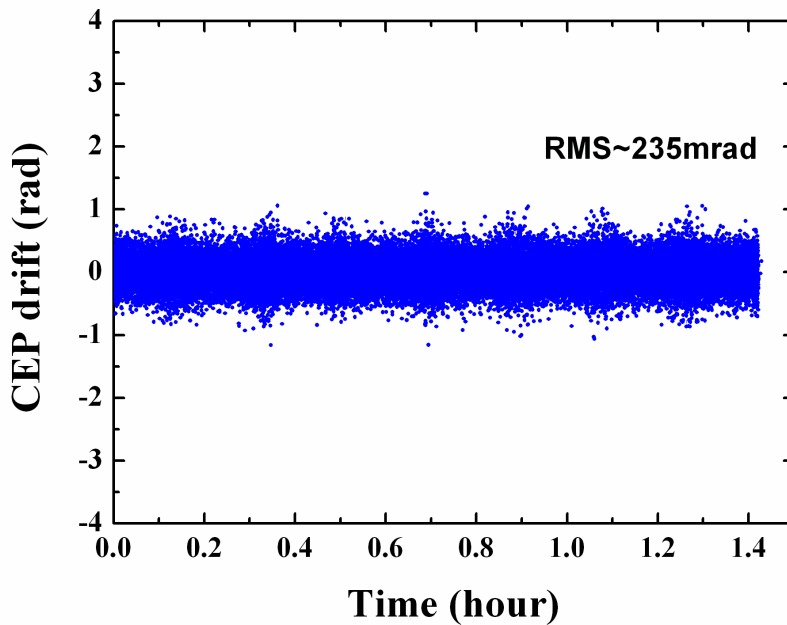


Figure 6.45: Closed loop CEP drift after spectral broadening in a hollow-core fiber and recompression.

6.11.5 Conclusions

In conclusion seeding the hollow fiber with circularly polarized pulses is a good solution to obtain a significant enhancement in energy throughput together with a notably improved spectral stability for circularly polarized seed pulses. Using this approach, 1 mJ, sub-5 fs pulses could be

generated, compressed from 2.5 mJ, 22 fs. Seeding larger core fibers with circularly polarized pulses should provide a effective way for generating sub-5fs pulses with even higher (multi-mJ) energies. This solution is the one adopted in our system for the generation of the energetic few-cycle pulses. As presented in the introduction the goal of the laser development of my group is to build an efficient (solid target) single attosecond source at high repetition rate (1 kHz). To obtain this source it is necessary to dispose of mJ level, CEP stabilized, kHz, few-cycle pulses. We can now satisfy these requirements. The ASE temporal contrast of our system is 10^7 which is enough to avoid pre-ionization of the target at least in the sub-relativistic regime. If the beam is taken directly after the hybrid compressor we also have a multi-mJ, 25 fs, kHz laser source for experiments in the multi-cycle regime. In the next chapter, after an introduction of the different regimes of high order generation on solid target, I will present the first experiments of laser-matter interaction with the study of the plasma mirror. In the last chapter of this thesis I present the future development of a double CPA system using an XPW contrast filter for obtaining ultra-high contrast pulses.

ï»¿

Bibliography

- [1] A. Baltuska, Z. Wei, M. S. Pshenichnikov, and D. A. Wiersma. Optical pulse compression to 5 fs at a 1-mhz repetition rate. *Opt. Lett.*, 22(2):102–104, 1997.
- [2] S. Bohman, A. Suda, M. Kaku, M. Nurhuda, T. Kanai, S. Yamaguchi, and K. Midorikawa. Generation of 5 fs, 0.5 tw pulses focusable to relativistic intensities at 1 khz. *Opt. Express*, 16(14):10684–10689, 2008.
- [3] R. W. Boyd. *NonLinear Optics*. Academic Press, Inc., 1992.
- [4] A. L Cavalieri, E. Goulielmakis, B. Horvath, W. Helml, M. Schultze, M. Fiess, V. Pervak, L. Veisz, V. S. Yakovlev, M. Uiberacker, A. Apolonski, F. Krausz, and R. Kienberger. Intense 1.5-cycle near infrared laser waveforms and their use for the generation of ultra-broadband soft-x-ray harmonic continua. *New Journal of Physics*, 9(7):242, 2007.
- [5] R. L. Fork, C. H. Brito Cruz, P. C. Becker, and C. V. Shank. Compression of optical pulses to six femtoseconds by using cubic phase compensation. *Opt. Lett.*, 12(7):483–485, 1987.
- [6] L. Gallmann, T. Pfeifer, P.M. Nagel, M.J. Abel, D.M. Neumark, and S.R. Leone. Comparison of the filamentation and the hollow-core fiber characteristics for pulse compression into the few-cycle regime. *Applied Physics B: Lasers and Optics*, 86(4):561–566, March 2007.
- [7] C. P. Hauri, M. Bruck, W. Kornelis, J. Biegert, and U. Keller. Generation of 14.8-fs pulses in a spatially dispersed amplifier. *Opt. Lett.*, 29(2):201–203, 2004.

- [8] C. P. Hauri, A. Trisorio, M. Merano, G. Rey, R. B. Lopez-Martens, and G. Mourou. Generation of high-fidelity, down-chirped sub-10 fs mj pulses through filamentation for driving relativistic laser-matter interactions at 1 khz. *Appl. Phys. Lett.*, 89(15):151125, Oct 2006.
- [9] C.P. Hauri, W. Kornelis, F.W. Helbing, A. Heinrich, A. Couairon, A. Mysyrowicz, J. Biegert, and U. Keller. Generation of intense, carrier-envelope phase-locked few-cycle laser pulses through filamentation. *Applied Physics B: Lasers and Optics*, 79(6):673–677, October 2004.
- [10] H. Mashiko, C. M. Nakamura, C. Li, E. Moon, H. Wang, J. Tackett, and Z. Chang. Carrier-envelope phase stabilized 5.6 fs, 1.2 mj pulses. *Applied Physics Letters*, 90(16):161114, 2007.
- [11] M. Nisoli, S. De Silvestri, and O. Svelto. Generation of high energy 10 fs pulses by a new pulse compression technique. *Applied Physics Letters*, 68(20):2793–2795, 1996.
- [12] M. Nisoli, S. Stagira, S. De Silvestri, O. Svelto, S. Sartania, Z. Cheng, M. Lenzner, C. Spielmann, and F. Krausz. A novel-high energy pulse compression system: generation of multi-gigawatt sub-5-fs pulses. *Applied Physics B: Lasers and Optics*, 65(2):189–196, August 1997.
- [13] M. Nurhuda, A. Suda, M. Kaku, and K. Midorikawa. Optimization of hollow fiber pulse compression using pressure gradients. *Applied Physics B: Lasers and Optics*, 89(2):209–215, November 2007.
- [14] S. Petit, A. Talebpour, A. Proulx, and S. L. Chin. Polarization dependence of the propagation of intense laser pulses in air. *Optics Communications*, 175(4-6):323 – 327, 2000.
- [15] S. Sartania, Z. Cheng, M. Lenzner, G. Tempea, Ch. Spielmann, F. Krausz, and K. Ferencz. Generation of 0.1-tw 5-fs optical pulses at a 1-khz repetition rate. *Opt. Lett.*, 22(20):1562–1564, 1997.
- [16] S. Stagira, E. Priori, G. Sansone, M. Nisoli, S. De Silvestri, and Ch. Gadermaier. Nonlinear guided propagation of few-optical-cycle laser pulses with arbitrary polarization states. *Phys. Rev. A*, 66(3):033810, Sep 2002.
- [17] G. Stibenz, N. Zhavoronkov, and G. Steinmeyer. Self-compression of millijoule pulses to 7.8 fs duration in a white-light filament. *Opt. Lett.*, 31(2):274–276, 2006.
- [18] J.H. Sung, J.Y. Park, T. Imran, Y.S. Lee, and C.H. Nam. Generation of 0.2-tw 5.5-fs optical pulses at 1 $\hat{\text{A}}$ khz using a differentially pumped hollow-fiber chirped-mirror compressor. *Applied Physics B: Lasers and Optics*, 82(1):5–8, January 2006.

- [19] A.J. Verhoef, J. Seres, K. Schmid, Y. Nomura, G. Tempea, L. Veisz, and F. Krausz. Compression of the pulses of a ti:sapphire laser system to 5 femtoseconds at 0.2 terawatt level. *Applied Physics B: Lasers and Optics*, 82(4):513–517, March 2006.
- [20] K. Yamakawa, M. Aoyama, S. Matsuoka, H. Takuma, C. P. J. Barty, and D. Fittinghoff. Generation of 16-fs, 10-tw pulses at a 10-hz repetition rate with efficient ti:sapphire amplifiers. *Opt. Lett.*, 23(7):525–527, 1998.
- [21] A. Zaïr, A. Guandalini, F. Schapper, M. Holler, J. Biegert, L. Gallmann, A. Couairon, M. Franco, A. Mysyrowicz, and U. Keller. Spatio-temporal characterization of few-cycle pulses obtained by filamentation. *Opt. Express*, 15(9):5394–5404, 2007.
- [22] E. Zeek, R. Bartels, M. M. Murnane, H. C. Kapteyn, S. Backus, and G. Vdovin. Adaptive pulse compression for transform-limited 15-fs high-energy pulse generation. *Opt. Lett.*, 25(8):587–589, 2000.